Human LDL core cholesterol ester packing: three-dimensional image reconstruction and SAXS simulation studies

Yuhang Liu, Dong Luo, and David Atkinson[1]

Department of Physiology and Biophysics, Boston University School of Medicine, Boston, MA 02118

Abstract **Human LDL undergoes a reversible thermal order-disorder phase transition associated with the cholesterol ester packing in the lipid core. Structural changes associated with this phase transition have been shown to affect the resistance of LDL to oxidation in vitro studies. Previous electron cryo-microscopy studies have provided image evidence that the cholesterol ester is packed in three flat layers in the core at temperatures below the phase transition. To study changes in lipid packing, overall structure and particle morphology in three dimensions (3D) subsequent to the phase transition, we cryo-preserved human LDL at a temperature above phase transition (53°C) and examined the sample by electron microscopy and image reconstruction. The LDL frozen from 53°C adopted a different morphology. The central density layer was disrupted and the outer two layers formed a "disrupted shell"-shaped density, located concentrically underneath the surface density of the LDL particle. Simulation of the small angle X-ray scattering curves and comparison with published data suggested that this disrupted shell organization represents an intermediate state in the transition from isotropic to layered packing of the lipid. Thus, the results revealed, with 3D images, the lipid packing in the dynamic process of the LDL lipid-core phase transition.**—Liu, Y., D. Luo, and D. Atkinson. **Human LDL core cholesterol ester packing: three-dimensional image reconstruction and SAXS simulation studies.** ***J. Lipid Res.*** **2011.** 52: **256–262.**

Supplementary key words low density lipoprotein • phase transition • atherosclerosis • electron cryo-microscopy • small angle X-ray scattering

LDL is a micro emulsion that transports lipid, mainly cholesterol ester, from liver to the peripheral tissues (1, 2). LDL particles are taken up by the cells through the LDL receptor and its cholesterol ester content enters the cell's metabolic pathways (3–5). When high levels of LDL accumulate in the circulation as a result of a deficiency in the LDL receptor, for example, the LDL can be oxidized and subsequentially interacts with macrophages. The accumulation of cholesterol ester transforms the macrophage into an atherogenic foam cell and contributes to the pathophysiology of atherosclerosis (6).

Previous studies have shown that the cholesterol ester in the core of the LDL particle can exist in two phases accompanying change in temperature (7–9). It also has been shown that the phase transition and lipid packing may affect the rate of LDL oxidation (10). Thus, the structure of the LDL lipid core has been intensively studied to shed light on its involvement in the processes of the early atherogenic events.

In the 1970s, a model for the cholesterol ester packing was proposed primarily based on X-ray and neutron scattering studies. These studies suggested that the cholesterol ester packed in concentric shells in the core at a temperature below the phase transition, and in an isotropic state at a temperature above the phase transition with the underlying assumption that the LDL is a spherical particle for both core phases (7–9, 11). More recent work from electron cryo-microscopy (cryo-EM) studies have shown in three-dimensional (3D) images that the LDL particle exhibits a disk shape instead of a sphere at temperatures below the phase transition, and the cholesterol ester forms a flat layered density (12–14) as opposed to concentric shells. However, the LDL lipid core structure above the phase transition, a more physiologically relevant state, remains controversial from image evidence. Two cryo-EM studies that attempted to freeze the LDL sample from a temperature above the phase transition have reached different conclusions about the changes of the cholesterol ester packing upon the phase transition (15, 16). This discrep-

This work was supported by grant NIH/NHLBI P0126335. Its contents are solely the responsibility of the authors and do not necessarily represent the official views of the National Institutes of Health.

Manuscript received 21 September 2010 and in revised form 1 November 2010.

Published, JLR Papers in Press, November 3, 2010
DOI 10.1194/jlr.M011569

Abbreviations: CTF, contrast transfer function; 2D, two dimensional; 3D, three dimensional; DPPC, 1,2-Dipalmitoyl-sn-glycero-3-phosphorylcholine; EM, electron microscopy; EYPC, egg yolk phosphorylcholine; SAXS, small angle X-ray scattering.

[1]To whom correspondence should be addressed.
e-mail: atkinson@bu.edu

ancy probably reflects the difficulty to capture the fast speed of this phase transition (17) and limitations of performing only two-dimensional (2D) projection image analysis because the LDL particle orientation and imaging defocus will affect the appearance of the striped images (12). In our previous studies (12), the core cholesterol ester layered packing was reliably observed in 3D image reconstructions of the structure of LDL prepared form a temperature lower than the phase transition. In the current studies, we fast-freeze LDL samples from a state above the phase transition and use 3D image reconstruction analysis to provide 3D image information for the LDL core structure that represents the state near physiological temperatures.

MATERIAL AND METHODS

Materials and chemicals

All the chemicals used in the experiments were standard and available from popular vendors. DPPC (1,2-Dipalmitoyl-sn-glycero-3-phosphorylcholine) was purchased from Matreya LLC. EYPC (L-α-Phosphatidylcholine ~99%) was purchased from Sigma. Electron microscope grids were QUANTIFOIL ®R 2/2 on 400 mesh Cu grids, which were purchased from Quantifoil Micro Tools (Jena Germany).

LDL preparation and characterization

Human LDL was isolated and a highly homogeneous subfraction of LDL was prepared and characterized following the procedures described before (12). Briefly, human plasma was prepared from blood of healthy nonfasting donors and treated with EDTA. LDL was separated from the plasma by ultracentrifugation floatation with the buoyant density range of 1.02–1.063 g/ml. This broad buoyant density range LDL was further fractionated with two rounds of KBr density gradient ultracentrifugation to get the final fractionated sample with the narrow buoyant density range between 1.035–1.04g/ml. The narrow density ranged LDL was dialyzed overnight against 10 mM phosphate, 150 mM sodium chloride, pH 7.4 buffer and used for the cryo-imaging experiments.

Lipid vesicle preparation

2.5 mg/ml lipid (DPPC or EYPC) in 10 mMol PBS buffer were sonicated for 5 min. During the sonication, the tube was immersed in the water bath to keep it in the desired temperature range (42°C for DPPC and ambient temperature for EYPC). After the sonication, the solutions were used for cryo-freezing experiments immediately.

Differential scanning calorimetry

Heat capacity $C_p(T)$ was measured with a MC2 microcalorimeter as described by Jayaraman et al. (18) LDL (apoB 2.0 mg/ml) in 10 mMol phosphate buffer was used as the sample and the dialysis buffer was used as the baseline reference. $C_p(T)$ was measured from 10°C to 60°C with a heating rate of 90K/h. After the first scan, the sample was cooled to 4°C, and another scan was repeated to examine the reversibility of the phase transition. The reference base line was subtracted from the sample curve in data analyses with the ORIGIN software.

Sample cryo-preservation at different temperatures

The cryo-preservation of the sample was performed in the Vitrobot® system. The sample cryo-preservation from 22°C was as described previously (12). LDL sample solution (4μl) was applied to the glow-discharged Quantifoil® Cu-400 mesh grid. The grid was incubated at 22°C in the chamber of the Vitrobot at a humidity of 100%. The grid was blotted and plunged into liquid ethane. The cryo-preservation from 53°C was preformed in the following way: the chamber temperature was set to 53°C and the chamber humidity was set to 100%. The tube holding the sample solution was placed inside of the chamber for about 10 min to reach the equilibrium state. Then, a discharge treated Quantifoil® Cu-400 mesh grid was placed inside the chamber and allowed to equilibrate for 2min. A pipetman was used to apply 4μl sample solution to the grid surface through a gated hole on the side wall of the chamber. After applying the sample, the incubation chamber was completely closed to the outside. The solution was allowed to settle on the grid for 1min and then the grid was blotted, plunged, and frozen in the liquid ethane cup below the chamber. The chamber gate that the grid traveled through did not open until this plunging process began. A custom-made taller ethane cup was used to hold the liquid ethane a few millimeters below the chamber gate and thus shortened the time that the sample grid was exposed to the cold air immediately above the liquid ethane. For the whole process, the sample stayed at 53°C no longer than 30 min. To make sure the changes at 53°C are associated only with the reversible lipid phase transition rather than protein degradation or particle fusion, the sample tube used for 53°C plunging was cooled in an ambient environment for 1 h and the LDL sample from this tube was frozen at 22°C again for comparison.

Cryo-EM and image processing

Images were collected on Tecnai TF20 electron microscope with an Oxford® cryo holder using low dose conditions. The defocus ranged from −1.2 um to −3.5 um. The data (except DPPC vesicles images) were collected with 29,000× magnification and recorded on a 4K TVIPS® CCD camera. The image file was at 2.9Å/pixel. For the DPPC vesicles images, the data were collected with 50,000× magnification and recorded on KODAK SO163 film. The films were digitized with a Creo EVERSMART® scanner and binned on a Linux computer. After binning, the image file was 2.73 Å /pixel.

For image reconstruction, particles images were picked with the *e2boxer* from EMAN2 program package (19), contrast transfer function (CTF) correction was performed with *ctfit* from the EMAN program package. The CTF corrected images were further binned to 5.46A/pix before structure reconstruction with the EMAN program (20).

The image reconstruction image results were displayed with the EMAN and Chimera (21) program packages.

SAXS calculation

The theoretical small angle X-ray scattering (SAXS) curve was calculated with a program modified from the SAXS module in the IMP package (22). First, density threshold values were chosen by properly displaying the desired internal feature of the LDL core in Chimera program (layered density for LDL from 22°, broken shell density for LDL from 53°C). To mimic a more disordered core structure, higher threshold values were given to the structure of LDL from 53°C to make the high density region in the core disappear in the displayed image. With these density threshold values, the modified program then defines the molecular composition regions within the LDL particle volume based on the voxel density values. All the voxels with a density value above the given threshold were designated as high electron density regions, which, in our model, represent the protein and the cholesterol ring moieties. All the voxels inside the LDL particle with a density value below the threshold was a low electron density

region, which, in our model, represents the acyl chains of the lipids. The averaged electron densities for LDL outer shell (poplar lipid head group and protein), cholesterol ring moieties and the acyl chains of the lipids are 0.38 e/Å^3, 0.42 e/Å^3, 0.29 e/Å^3 respectively (7). Water has an averaged electron density of 0.33 e/Å^3. Thus, the form factors for high and low density regions were given values of 1 and −0.5, respectively, to reflect the electron density differences of the outer shell, cholesterol ring regions, and the disordered acyl chain regions from the lipids compared with the water in the buffer solution. With the defined form factors and the 3D coordinates, each individual voxel was considered as a particle and used in the theoretical SAXS calculations based on the Debye formula (22).

RESULTS

LDL exhibits a reversible phase transition

Figure 1 shows the LDL heat capacity C_p (T) as a function of temperature. The sample was heated from 10°C to 60°C (dots). The curve showed a peak that started at ~22°C and ended at ~36°C. This peak represents the phase transition of the cholesterol ester in LDL core (8). After the sample reached 60°C, it was cooled to 4°C and heated again to 60°C (solid line). The second curve overlapped with the first, demonstrating that the sample underwent a reversible phase transition over this temperature range.

DPPC vesicles as a freezing speed monitor

DPPC vesicles were preserved at 22°C and 53°C following the cryo-freezing conditions described. As shown in **Fig. 2A,** when preserved from 22°C, the vesicles showed a faceted shape. When the DPPC vesicles were preserved from 53°C, the vesicles mostly showed a smooth round shape (Fig. 2B). This smooth shape morphology of the DPPC vesicles was comparable to the EYPC vesicles frozen from 22°C (Fig. 2C) [the major component of EYPC has a phase transition temperature below 0°C and the acyl chain is preserved in a fluid state (23)].

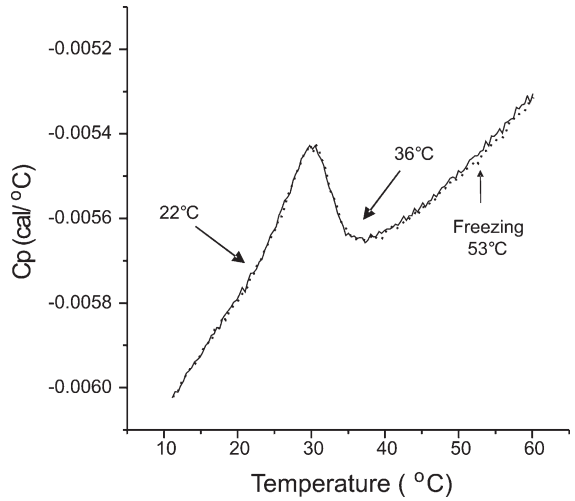

Fig. 1. Reversible phase transition of LDL. Heat capacity $C_p(T)$ as a function of temperature collected from 10°C to 60°C (dots). After reaching 60°C, the sample was cooled to 4°C and the heating process was repeated (solid line). The sample has a lipid-core phase transition between ~22°C to ~36°C. The temperature at which we performed the freezing above the phase transition was indicated (53°C).

Projection image, 2D classification, 3D reconstruction comparisons

As shown in **Fig. 3**, the EM projection images of LDL frozen from 22°C showed a characteristic striped feature. These stripes are thought to be produced from the layered cholesterol ester packing and are most often observed as continuous parallel lines with similar distance of ~32Å between the lines. For the LDL sample frozen from 53°C, the internal density of the particles was observed to be in a disrupted line or a circular shape. When the same sample was cooled to 22°C and frozen, the straight parallel stripes became clear again and the circular density in the LDL particle was not seen.

Approximately 9,000 particles were selected from electron micrographs of LDL samples prepared from each of the three conditions. The 2D images of these particles were classified and averaged with the initial reference free *refine2d.py* program from EMAN package (20). Top five class average images with the clearest features inside the particle from each condition are shown for comparison in **Fig. 4A**. The LDL frozen from 22°C had strong, straight, striped features, whereas for the LDL prepared from 53°C, only weak, straight, striped features were observed in two class average images. The dominant density feature inside of the particle was circular in shape. The particles with the circular density inside also exhibited a smooth oval shape as opposed to the more rectangular shape observed at 22°C. The total number of particles in the class averages that exhibited clear inside high density features was summed as shown in Fig. 4B.

Three-dimensional structure reconstructions were performed for the three datasets with the EMAN program (20). The resolutions for each reconstruction were determined with FSC = 0.5 cutoff using *eotest* program in the EMAN package as the following: LDL from 22°C: 28Å; LDL from 53°C: 31Å; LDL cooled back to 22°C: 28Å. The lipid core structures of LDL from each condition are compared in **Fig. 5A**, in which the structure volumes were sliced with the plane perpendicular to the lipid layer structure, and in Fig. 5B, in which the structure volumes were sliced with the plane parallel to the lipid layer at five levels. The positions of the cutting planes are indicated in Fig. 5C. The LDL core structures from 22°C all showed three planar layers of density (Fig. 5A, B). The LDL core structure from 53°C showed a "disrupted shell"-like density, and the central layer density was largely disrupted (Fig. 5A, B). The LDL particle from 53°C exhibited a more "spherical" morphology, which can be seen in Fig. 5A.

SAXS calculation for the models

The theoretical SAXS curve from the structure with the "layered core" showed a peak at around **s**=0.03 (Å^{-1}). The disrupted shell structure showed decreased peak intensity in this region. As the density feature inside gradually

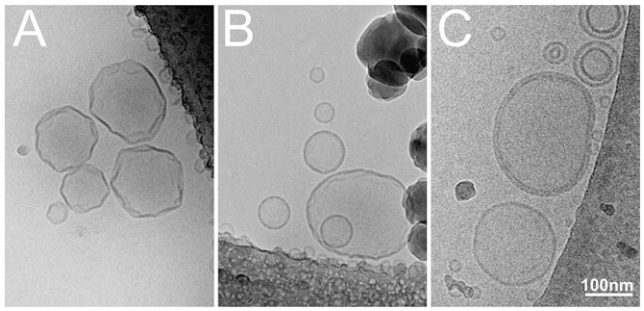

Fig. 2. Phospholipids vesicles as cryo-freezing speed monitor. A: DPPC vesicles frozen from 22°C. B: DPPC vesicles frozen from 53°C under the conditions described in Methods. C: EYPC vesicles frozen from 22°C.

disappeared in the core of LDL by varying the density threshold, the peak at **s**=0.03 ($Å^{-1}$) became weaker until almost absent. The disappearance of this peak was consistent with the shape function that dominants the scattering (**Fig. 6**).

DISCUSSION

Recent work has shown that the phase transition of the LDL lipid core occurs over a timescale in the range of ~10ms (17). Thus, it presents a challenge to freeze the cryo-EM grid and preserve the LDL sample in a state above phase transition. In the cryo-EM grid freezing process, although the liquid ethane can freeze the sample solution in ~1ms (24), the EM grid will inevitably travel through a cold zone that exists above the liquid cryogen. As a result, the EM grid and the sample solution may experience a sub-phase transition temperature in the air for a few milliseconds before being cryo-frozen. The total time that the sample experiences a sub-phase transition temperature may be close to the lipid phase transition time of LDL. With this issue in mind, we attempted to minimize the time that the sample grid experienced a sub-phase transition temperature before being frozen: The incubation chamber was set at 53°C, which is ~16°C above the point that the LDL lipid core goes from a disordered to an ordered state (Fig. 1). [The LDL particle is stable and free from thermal denaturation at this temperature for a period of time (18).] The distance between the ethane surface and the 53°C chamber was minimized to a few millimeters and the door separating them only opened ~2 s before the grid was plunged in the liquid ethane. Freezing speed was tested with the DPPC vesicles. The acyl chains of a DPPC molecule have a fluid-solid phase transition at the temperature of ~41°C (23). When we froze the lipid vesicles from 22°C, the vesicles adopted a faceted morphology suggesting that the acyl chains of the DPPC molecules are in the solid phase (Fig. 2A). When we froze the lipid vesicles from 53°C with our procedures, the DPPC vesicles had a smooth curvature (Fig. 2B). This smooth curvature is similar to the curvature of EYPC vesicles (Fig. 2C) for which the acyl chains are in the liquid phase (23). Thus, our plunge freezing setting at 53°C is fast enough to capture the liquid state of the acyl chain of the DPPC molecules. This phase transition happens in the time scale of ~9ms (24) which is comparable to the timescale of the LDL lipid core phase transition (17).

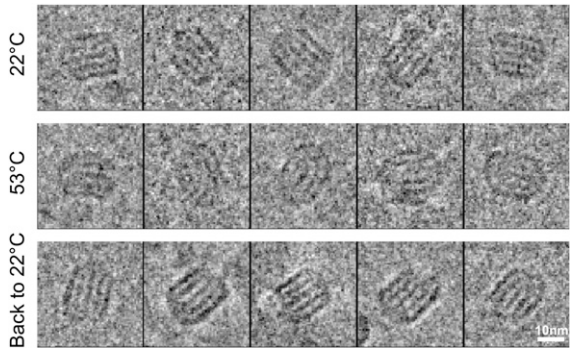

Fig. 3. Comparison of projection images of LDL particles obtained by freezing from 22°C, 53°C, and 22°C after heating. The darker areas represent the higher electron density regions in the images.

Projection images with high densities inside were compared for images taken at defocus ~1.8um, at which the striped feature is most visible. In LDL frozen from 22°C, the characteristic striped particles were clear. The stripes inside the particles were continuous and straight, and often extended from one side to the other (Fig. 3). In contrast, for the LDL frozen from 53°C, such striped particles were observed less often (Fig. 4B) and the images showed disrupted electron densities as dark regions inside the particles (Fig. 3). These densities did not form parallel lines and in some cases formed a circle concentric with the outermost layer of the LDL particle (the third image). These images may capture an intermediate state between the disorder-order phase transition of the individual particles (see state determination from the SAXS curve simulation later in discussion). The densities inside the particle may represent the nano-environment that is enriched in certain lipids due to the molecular level interactions (1). When the sample was cooled, the characteristic stripes became clear again (Fig. 3).

Particles from each freezing condition were selected and subjected to 2D classification and 3D image reconstruction. In the 2D classification, for the sample frozen from 22°C, the electron density formed continuous straight lines that were parallel to each other and the particle's flat surface (Fig. 4A). On the other hand, the class average images from 53°C showed some images with circular shape density in the core that was concentric with the surface of the LDL particle. In addition, the particle shape was smoother and was more circular in morphology (Fig. 4A). The class average images with internal density that was in circular shape were only observed in the LDL frozen from 53°C and the particles that were classified into the circular density class were dominant (Fig. 4B).

The 3D image reconstructions revealed the difference in core structure between the samples frozen from 22°C and 53°C. In the sample prepared from 22°C, the lipid core always exhibited the layered organization (Fig. 5A, B). However, for the sample prepared from 53°C, the cen-

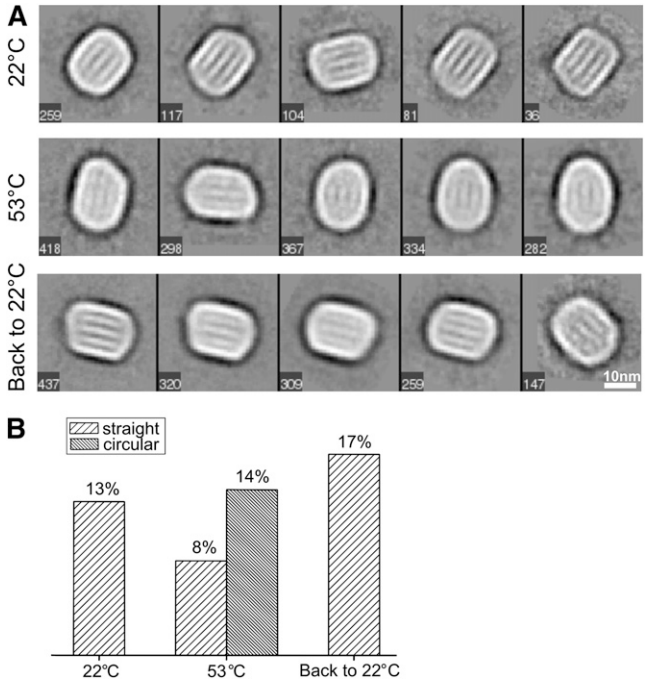

Fig. 4. Comparison of 2D projection class averaged images of LDL obtained by freezing from 22°C, 53°C, and 22°C after heating. Top five class averaged images that clearest show high electron density inside of the particle from each condition. The number of particles contained in that class is indicated on the lower left. The lighter areas represent the higher electron density regions in the images. A: Class averaged images from the three conditions. B: Percentages of the particles that contained in the classes, which showed high density features inside LDL particle in the class average image in the three conditions.

tral density layer largely disappeared and the upper and lower layers were curved and connected to form a disrupted shell- like structure. This disrupted shell structure was concentric with the surface of LDL particle and the distance of the shell was about the same as that for the layers to the surface in LDL frozen from 22°C (Fig. 5A, B). This core structure was consistent with the results in the projection images (Fig. 3) and the 2D class average (Fig. 4A). Thus, the shell-like arrangement of the core represents the structure from the major population of the particles in the image data set rather than an averaged result of the two (layered and isotropic) populations. The reappearance of the straight lines in 2D images and flat layers in 3D structures after cooling suggests the structure changes observed in the images from 22°C to 53°C are reversible and are attributed to the lipid phase transition.

To determine the temperature ranges that these different structured LDL experienced during freezing, we calculated the theoretical SAXS curve from the structures as shown in Fig. 6. The calculated SAXS curves showed close similarities in shape with the experimental curves (7, 8, 11), which validates that the calculation program can reflect the electron density geometry from the structure volume properly. The SAXS curves for the layered structure showed a strong maximum at ~**s**=30Å^{-1}. The SAXS curves for the disrupted shell structure showed a peak at the same **s** value, but the intensity of the peak was dramatically decreased. This intensity change may largely result from the missing central layer, without which the ~32Å spacing repeats of the high density between the cholesterol ring moieties are disrupted (12). The intensities at this **s** value from the disrupted shell structure closely resemble the experimental SAXS data of LDL at temperatures between the beginning and the peak temperature during the order-disorder phase transition process (8). This remaining peak probably reflects the geometry between the disrupted shell and the LDL particle surface. We varied the density threshold of the LDL structure volume from 53°C to decrease the high density features inside the LDL particle to mimic a more disordered state of the core lipid. As the density threshold changed and the core density disappeared, the peak at ~**s**=30Å^{-1} in the SAXS curve also decreased corre-

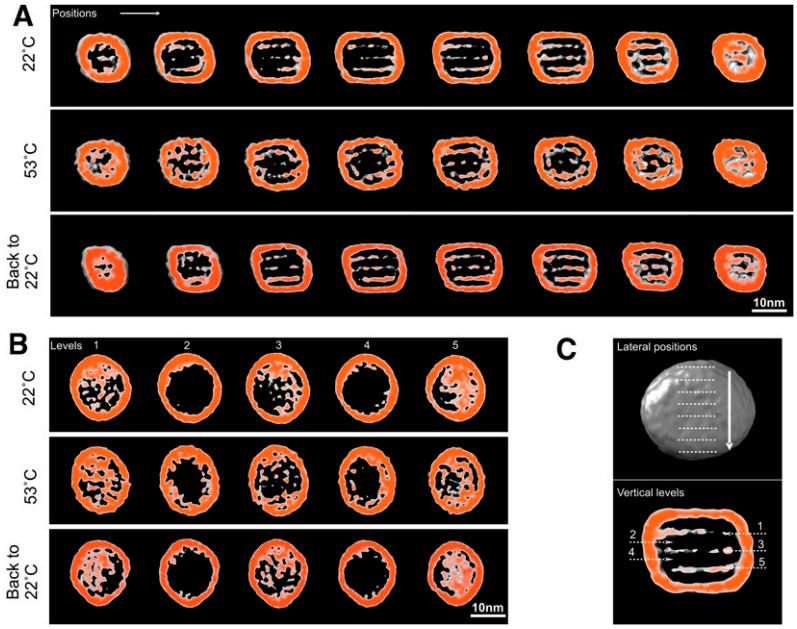

Fig. 5. Comparison of the internal features of the reconstructed 3D volume of LDL prepared from 22°C, 53°C, and 22°C after heating. The volumes of the different reconstructions were aligned and the volumes were sliced to reveal the internal structure of the particles. The gray color was contoured at 2σ and the orange color was contoured at 3σ. Images were displayed with the Chimera program (21). A: The structure of the LDL lipid core revealed with slices perpendicular to the lipid layers. B: The structure of the LDL lipid core revealed with slices parallel to the lipid layers at five levels. The positions of the slices are indicated in C.

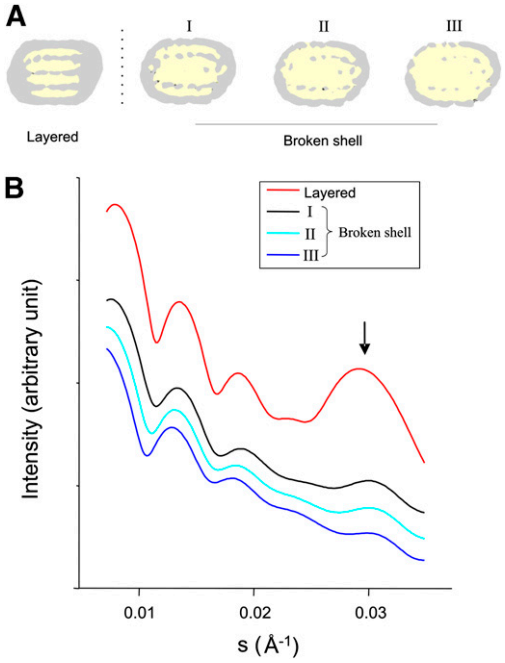

Fig. 6. Calculated SAXS curve from the 3D structures. A: Defining the form factor for two density regions. The gray regions are high electron density regions and defined to have a form factor of 1, and the yellow regions are low electron density regions and defined to have a form factor of -0.5. In broken shell volume, to decrease the high density regions in the lipid core, different thresholds were chosen **I** < **II** < **III**. B: Calculated SAXS curve. **s**=2sinθ/λ (2θ is the scattering angle and λ is the X-ray wavelength). Arrow indicate the peaks at around **s**=0.03 that resembles the experimental data (8).

spondingly and became almost absent when the high density in the "shell" shape was barely visible. The disappearance of the peak intensity in the simulated SAXS curve is similar to experimental data for LDL at the temperatures above the peak of the phase transition (8). Thus, the lipid packing states reflected in the 3D images are linked to the temperature ranges in the phase transition process as shown in **Fig. 7**. Above the peak phase transition temperature(>∼30°C), the cholesterol esters are isotropically organized, as the temperature decreases, the cholesterol esters start to nucleate in patches, probably through the interaction with the acyl chain part of phospholipid monolayer at the LDL particle surface. The interactions between the steroid rings may form and the cholesterol esters are arranged in the shell like structure. As the temperature continues to drop (<∼22°C), the cholesterol ester molecules inside the disrupted shell may form the central layer through the interaction with the acyl chain of the cholesterol esters that already exist in the shell-like arrangement. The transition process is completed in a milliseconds time scale. This core-lipid phase transition also has an impact on the overall shape of LDL particle, which is evidenced by the subtle change in LDL particle shape (Figs. 4, 5).

Although we initially designed the cryo-EM experiments to search for image evidence of the lipid packing at a state above the phase transition temperature, we found that the images are more consistent with LDL particles mostly ex-

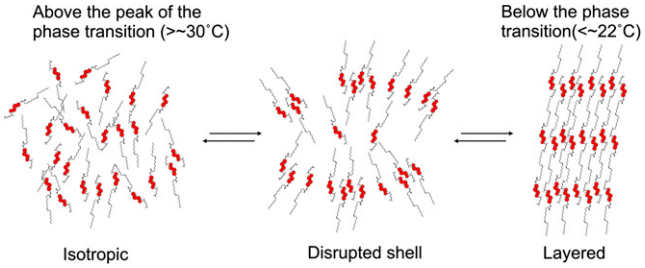

Fig. 7. Dynamic model of the LDL core cholesterol esters packing during phase transition. The cholesterol ester molecules are drawn and the sterol ring part is highlighted in red. The dynamic change in CE packing during phase transition is depicted from left to right. Isotropic ↔ Disrupted shell↔ Layered. Corresponding temperature states are indicated.

isting in an intermediate state during the phase transition process. These observations suggest that, despite of our efforts to optimize the freezing conditions, the onset of the LDL core disorder-order phase transition takes place faster than the cryo-freezing speed of the current setup. However, the observation of an intermediate state supplements the existing two states phase transition model and reveals the dynamic process of lipid nucleation from isotropic to layered packing during the lipid-core phase transition. This lipid phase transition also introduced a morphological change in the LDL particle, which may be related to the properties at the particle surface such as subtle changes in protein conformation and the LDL particle surface pressure and may partially account for the different resistance to oxidation for LDL at different temperatures (10). In the body, as LDL particles circulate to the peripheral tissues, they may experience temperatures ranges in which the phase transition occurs (25). Thus, the structure changes that have been shown in our study are relevant in vivo conditions. The effects of this phase transition induced structural changes in LDL on the interaction with other molecular players wait further investigation.

The authors thank Cheryl England and Michael Gigliotti for their help in preparing the LDL samples. We thank Dr. Jean-François Ménétret for the help during the experiments. We thank Dina Schneidman and Andrej Sali at University of California, San Francisco for the help in SAXS calculation.

REFERENCES

1. Hevonoja, T., M. O. Pentikainen, M. T. Hyvonen, P. T. Kovanen, and M. Ala-Korpela. 2000. Structure of low density lipoprotein (LDL) particles: basis for understanding molecular changes in modified LDL. *Biochim. Biophys. Acta.* **1488:** 189–210.
2. Mahley, R. W., T. L. Innerarity, S. C. Rall, Jr., and K. H. Weisgraber. 1984. Plasma lipoproteins: apolipoprotein structure and function. *J. Lipid Res.* **25:** 1277–1294.
3. Brown, M. S., and J. L. Goldstein. 1974. Familial hypercholesterolemia: defective binding of lipoproteins to cultured fibroblasts associated with impaired regulation of 3-hydroxy-3-methylglutaryl coenzyme A reductase activity. *Proc. Natl. Acad. Sci. USA.* **71:** 788–792.
4. Brown, M. S., and J. L. Goldstein. 1979. Receptor-mediated endocytosis: insights from the lipoprotein receptor system. *Proc. Natl. Acad. Sci. USA.* **76:** 3330–3337.

5. Goldstein, J. L., and M. S. Brown. 1976. The LDL pathway in human fibroblasts: a receptor-mediated mechanism for the regulation of cholesterol metabolism. *Curr. Top. Cell. Regul.* **11:** 147–181.
6. Watkins, H., and M. Farrall. 2006. Genetic susceptibility to coronary artery disease: from promise to progress. *Nat. Rev. Genet.* **7:** 163–173.
7. Atkinson, D., R. J. Deckelbaum, D. M. Small, and G. G. Shipley. 1977. Structure of human plasma low-density lipoproteins: molecular organization of the central core. *Proc. Natl. Acad. Sci. USA.* **74:** 1042–1046.
8. Deckelbaum, R. J., G. G. Shipley, and D. M. Small. 1977. Structure and interactions of lipids in human plasma low density lipoproteins. *J. Biol. Chem.* **252:** 744–754.
9. Laggner, P., G. M. Kostner, G. Degovics, and D. L. Worcester. 1984. Structure of the cholesteryl ester core of human plasma low density lipoproteins: selective deuteration and neutron small-angle scattering. *Proc. Natl. Acad. Sci. USA.* **81:** 4389–4393.
10. Schuster, B., R. Prassl, F. Nigon, M. J. Chapman, and P. Laggner. 1995. Core lipid structure is a major determinant of the oxidative resistance of low density lipoprotein. *Proc. Natl. Acad. Sci. USA.* **92:** 2509–2513.
11. Prassl, R., B. Schuster, P. M. Abuja, M. Zechner, G. M. Kostner, and P. Laggner. 1995. A comparison of structure and thermal behavior in human plasma lipoprotein(a) and low-density lipoprotein. Calorimetry and small-angle X-ray scattering. *Biochemistry.* **34:** 3795–3801.
12. Liu, Y., and D. Atkinson. 2010. Enhancing the contrast of apoB to locate the surface components in the 3D density map of human LDL. *J. Mol. Biol.* **405:** 274–283.
13. Orlova, E. V., M. B. Sherman, W. Chiu, H. Mowri, L. C. Smith, and A. M. Gotto, Jr. 1999. Three-dimensional structure of low density lipoproteins by electron cryomicroscopy. *Proc. Natl. Acad. Sci. USA.* **96:** 8420–8425.
14. Ren, G., G. Rudenko, S. J. Ludtke, J. Deisenhofer, W. Chiu, and H. J. Pownall. 2010. Model of human low-density lipoprotein and bound receptor based on cryoEM. *Proc. Natl. Acad. Sci. USA.* **107:** 1059–1064.
15. Coronado-Gray, A., and R. van Antwerpen. 2005. Lipid composition influences the shape of human low density lipoprotein in vitreous ice. *Lipids.* **40:** 495–500.
16. Sherman, M. B., E. V. Orlova, G. L. Decker, W. Chiu, and H. J. Pownall. 2003. Structure of triglyceride-rich human low-density lipoproteins according to cryoelectron microscopy. *Biochemistry.* **42:** 14988–14993.
17. Prassl, R., M. Pregetter, H. Amenitsch, M. Kriechbaum, R. Schwarzenbacher, J. M. Chapman, and P. Laggner. 2008. Low density lipoproteins as circulating fast temperature sensors. *PLoS ONE.* **3:** e4079.
18. Jayaraman, S., D. Gantz, and O. Gursky. 2005. Structural basis for thermal stability of human low-density lipoprotein. *Biochemistry.* **44:** 3965–3971.
19. Tang, G., L. Peng, P. R. Baldwin, D. S. Mann, W. Jiang, I. Rees, and S. J. Ludtke. 2007. EMAN2: an extensible image processing suite for electron microscopy. *J. Struct. Biol.* **157:** 38–46.
20. Ludtke, S. J., P. R. Baldwin, and W. Chiu. 1999. EMAN: semiautomated software for high-resolution single-particle reconstructions. *J. Struct. Biol.* **128:** 82–97.
21. Goddard, T. D., C. C. Huang, and T. E. Ferrin. 2005. Software extensions to UCSF chimera for interactive visualization of large molecular assemblies. *Structure.* **13:** 473–482.
22. Schneidman-Duhovny, D., M. Hammel, and A. Sali. 2010. FoXS: a web server for rapid computation and fitting of SAXS profiles. *Nucleic Acids Res.* **38(Suppl):** W540–544.
23. Small, D. M. 1986. The physical chemistry of lipids from alkanes to phospholipids. *In* Handbook of Lipid Research. D. J. Hanahan, editor. Plenum, New York. 475–522.
24. Siegel, D. P., W. J. Green, and Y. Talmon. 1994. The mechanism of lamellar-to-inverted hexagonal phase transitions: a study using temperature-jump cryo-electron microscopy. *Biophys. J.* **66:** 402–414.
25. Burton, A. 1935. Human calorimetry: the average temperature of the tissues of the body. *J. Nutr.* **9:** 261–280.